Phase locking and frequency doubling in spin-transfer-torque oscillators with two coupled free layers

Takahiro Moriyama,[1] Giovanni Finocchio,[2] Mario Carpentieri,[3] Bruno Azzerboni,[2] Daniel C. Ralph,[1,4] and Robert A. Buhrman[1]

[1]*Cornell University, Ithaca, New York 14853 USA*
[2]*Department of Fisica della Materia e Ingegneria Elettronica, University of Messina, C. da di Dio, I-98166 Messina, Italy*
[3]*Department of Elettronica, Informatica e Sistemistica, University of Calabria, Via P. Bucci 42C, I-87036 Rende (CS), Italy*
[4]*Kavli Institute at Cornell, Cornell University, Ithaca, New York 14853, USA*

We report measurements of spin-torque-driven oscillations in magnetic multilayer devices containing two in-plane-oriented free layers designed to have significant coupling between them. They are driven to oscillate by spin-transfer torque from two perpendicularly oriented polarizers. For both measured devices and micromagnetic simulations, we find that the oscillations in the two free layers are phase locked, resulting in a frequency doubling and large output signals. The simulations suggest that the oscillations are due to spatially nonuniform dynamics characterized by coupled large-amplitude motion of the two free layers.

Spin-transfer-torque oscillators (STOs) have the potential to serve as nanoscale microwave-frequency sources and detectors.[1–7] In order for STOs to be promising candidates for applications, one must optimize simultaneously a variety of properties, including operation to high frequencies, frequency tunability, narrow spectral linewidth, large output power, and operation in the absence of an external magnetic field. Different strategies have been demonstrated for optimizing subsets of these properties. For example, spin-torque-driven gyration of magnetic vortices can provide relatively narrow linewidths and operation in zero magnetic field,[8–11] but the output frequency is limited to values smaller than 1 GHz. Reductions of the linewidth and increases in the output power can be realized by phase locking the dynamics of several STOs.[11–13] The output power can also be increased by employing magnetic tunnel junctions with large magnetoresistance.[5,6] Here we explore a strategy that may have the potential to help achieve simultaneously higher-frequency operation, a large magnetic precession angle, narrowed spectral linewidth, and zero-field operation, by employing a device geometry with two magnetic free layers coupled together to achieve phase locking of their dynamics. Our measurements show that the two free layers can undergo spin-torque-driven large-angle phase-locked precession at zero field, in a mode having the property that the frequency of the resistance signal is twice the magnetic precession frequency. Micromagnetic simulations indicate that this coupled mode involves spatially inhomogeneous magnetic dynamics within each of the two free layers, and that because of the interlayer coupling the two-free-layer geometry should yield reduced oscillator linewidths compared to analogous devices with a single free layer.

Our multilayer samples [Fig. 1(a)] are deposited using magnetron sputtering onto oxidized Si wafers and have the structure buffer layer/[Co/Pt] polarizing layer/Cu (2)/Co (4) free layer #1/Cu (4)/Co (4) free layer #2/Cu (2)/[Co/Ni] polarizing layer/capping layers, where the numbers in parentheses are thicknesses in nm. The Co/Pt and Co/Ni polarizing layers are designed to have perpendicular magnetic anisotropy; they have the structures [Co (0.5)/Pt (2)]$_4$/Co (0.6) and [Co (0.2)/Ni (0.8)]$_8$ (see details about the fabrication methods

in the Supplemental Material[14]). We pattern the film into nanopillars with an elliptical cross section (170×130 nm^2) using electron-beam lithography and Ar ion milling [Fig. 1(b)], prior to top electrode deposition.

To characterize the samples, we measure the magnetization of unpatterned films and the magnetoresistance (MR) of patterned devices while applying magnetic fields out of the sample plane (H_{op}) and in plane along the long axis of the ellipse (H_{ip}). The magnetization measurements on the unpatterned film [Fig. 1(c)] show, as expected, that the sample has both in-plane and out-of-plane components of magnetic anisotropy. The ratio between in-plane and out-of-plane components of the remanent magnetization is found to be 1.3, which agrees well with the ratio of the moments between the in-plane oriented layers (the two Co free layers) and the perpendicularly oriented Co/Pt and Co/Ni polarizer layers. In the magnetoresistance curves [Fig. 1(d)], the resistance jumps of $\Delta R = 0.2$ Ω for in-plane applied fields are associated with switching of the in-plane-oriented Co layers. Based on the switching fields in the major and minor loops, we estimate that the anisotropy field of the Co layers is ∼180 Oe and the dipolar field strength between the Co layers is ∼320 Oe favoring antiparallel alignment.

To prepare for measuring the microwave output of these oscillators, we apply a strong magnetic field $H_{op} > 6$ kOe so that both perpendicular polarizers align in $+z$ direction, and then we ramp the field to zero. We record the microwave power spectral density (PSD) transmitted via a 50 Ω coplanar waveguide probe while we sweep the dc bias current (I_{dc}) from zero toward either positive or negative values. Positive current is defined as the sign for which electrons flow from the bottom of the device to the top. We have measured five different samples with the same nominal 170×130 nm^2 elliptical cross section. The microwave output properties did vary somewhat between devices (as noted below), but the phenomena we will emphasize here were present in all five devices. All the data we will present are from a single device, measured at room temperature.

In Fig. 2 we plot the PSD and the dc resistance as a function of I_{dc} for zero external magnetic field. Microwave
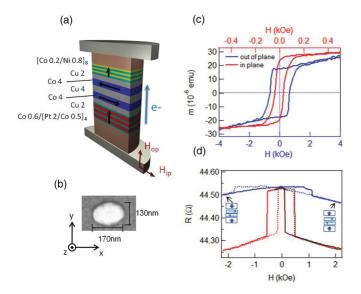
FIG. 1. (Color online) (a) Schematic of the nanopillar device geometry. H_{op} and H_{ip} indicate the directions of the positive out-of-plane and in-plane magnetic fields. (b) Top view of the nanopillar before depositing the top electrode, as viewed by a scanning electron microscope. (c) Magnetization curves of a large-area multilayer sample for magnetic field applied out of plane (blue) and in plane (red). (d) Magnetoresistance curves for a nanopillar device for magnetic field applied out of plane (blue) and in plane (red) near zero current (500 μA). The dotted curves are scans from the positive to the negative field and the solid curves are the reverse scans. The black curves represent a minor loop.

oscillations are observed for both current directions starting near $I_{dc} = \pm 3.8$ mA, with the frequencies decreasing slightly with increasing $|I_{dc}|$. This dependence disagrees with the prediction of a simple macrospin model for an in-plane free
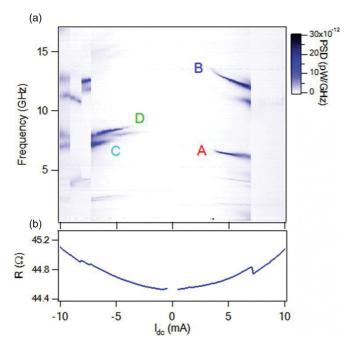

FIG. 2. (Color online) (a) The measured microwave PSD as a function of the current bias at zero external field. (b) The associated dc resistance.

layer/perpendicular polarizer sample for which one would expect the frequency to increase with $|I_{dc}|$.[15] At positive current we observe a strong fundamental peak (A) near 6.5 GHz and a second harmonic (B) near 13 GHz, while at negative current we measure two closely spaced peaks (C and D) near 7.5 GHz. When the current is increased beyond $I_{dc} = +7.0$ mA the strong microwave output ceases abruptly and the dc resistance [see Fig. 2(b)] undergoes a sudden drop. However, when the current is swept to large magnitudes in the negative direction, for $I_{dc} < -7.4$ mA, the dynamics do not cease, instead they undergo a sequence of transitions into different modes with smaller powers. In comparing the different samples, all five samples that we measured had similar dynamics for positive current, but for negative currents where the dynamics are more complicated there were greater differences. In the analysis below, we will focus on the reproducible behaviors we observe at positive bias. Micromagnetic simulations suggest that the differences as a function of current polarity may be associated with asymmetries in the dipole fields and the spin torques from the different perpendicular polarizing materials, and it is also possible that dynamics might be excited at negative bias in the Co/Ni polarizer as well as the Co free layers.[16,17]

Figure 3 summarizes the experimental results as a function of I_{dc} at positive bias for (a) the precession frequency, (b) the PSD peak heights, and (c) the linewidths for the fundamental peak A and second harmonic peak B. The maximum integrated powers P are equivalent to peak-to-peak resistance oscillations $\Delta R_{pp} = 4[2RP]^{1/2}/I_{dc} = 0.014$ Ω for peak A and 0.016 Ω for peak B, which are $\sim$7%–8% of the full resistance change ($\Delta R = 0.2$ Ω) upon switching between parallel and
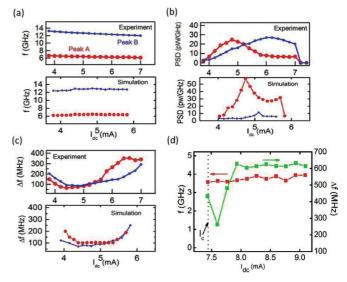

FIG. 3. (Color online) (a) The peak frequency, (b) power spectral density, and (c) linewidth for the fundamental peak A (large red circles) and the second harmonic B (small blue circles) as a function of I_{dc}. The upper panels in (a), (b), and (c) show the experimental data and the lower panels are the results of the micromagnetic simulations at room temperature (300 K). (d) The results of room-temperature micromagnetic simulations for the single-free-layer spin valve geometry described in the text, for the frequency and the linewidth corresponding to oscillations of the average x component of the free layer magnetization.

antiparallel configurations of the two free layers. (In deriving this estimate we use that our sample resistance and the transmission line impedance are both approximately $R = 50\,\Omega$.)

To identify the nature of the persistent magnetization oscillations, we performed micromagnetic simulations.[14,18,19] We solved the Landau-Lifshitz-Gilbert-Slonczewski (LLGS) equation to model the magnetic dynamics of the two Co free layers while assuming that the magnetizations of the perpendicular polarizers remain fixed. We use typical experimental parameters for Co together with an in-plane magnetic anisotropy $K_u = 1.26 \times 10^4\,\text{J/m}^3$ so that the switching fields are consistent with experiment. We make the rough approximations that the spin polarizations of the various magnetic layers are 0.15 for Co/Pt,[20] 0.3 for Co/Ni,[21] and 0.36 for Co.[20,22] With these model parameters, the calculated critical currents for spin-torque-driven excitations are in good agreement with the experiment (see Fig. 3), although the current range over which persistent magnetization oscillations exist is about 40% smaller in the simulation. We consider this to be very reasonable agreement given the level of uncertainty about experimental parameters such as the spin polarizations for the different layers.

We performed systematic simulations of the magnetoresistance signal as a function of current, at both zero temperature and room temperature. Figure 4 shows results of a zero-temperature micromagnetic simulation for $I_{dc} = 5.3$ mA. The power spectra for the magnetization oscillations of the free layers [Fig. 4(a)] indicate that the magnetic precession frequency for both layers is 3.1 GHz. However, there is no peak in the PSD of the simulated resistance oscillations at

3.1 GHz—the lowest frequency present in the MR oscillations is twice that, at 6.2 GHz. The time traces of the averaged x and y components of the averaged magnetization for the top and the bottom free layers are displayed in Fig. 4(b) together with the time trace of the total sample resistance. Despite the fact that the spin torques exciting the two layers are different, we find that the two layers are phase locked to oscillate at the same frequency (3.1 GHz), with a nonzero relative phase. The relative motion of the two layers results in a time-dependent resistance oscillating at twice the precession frequency. The mechanism behind the frequency doubling can be understood based on snapshots of the magnetization configurations at different times in the precessional cycle [Fig. 4(c)]. The magnetization dynamics in both free layers are spatially nonuniform, with the exact dynamics differing between the two layers. However, there is a symmetry in the configurations when comparing time points differing by half a precessional period [e.g., times t_1 and t_4 in Fig. 4(c)], that the magnetization configuration in each layer is related by a $180°$ rotation about the $\hat{z}$ axis between the two time points, so that the relative configurations of the two layers (and hence the resistance) are the same. We therefore identify the cause of the frequency doubling as a natural consequence of phase locking between the two magnetic free layers.

The simulations indicate that this phase locking arises from the combined effect of both magnetostatic coupling between the free layers and coupling by means of the spin-transfer torque due to current flow between the layers—phase locking is not observed when either of these coupling mechanisms is removed from the simulations. As the current is increased in the simulations, there is a critical value of ~5.9 mA where the resistance oscillations cease, in a way qualitatively similar to experiment. In the simulations, this occurs because a static magnetic vortex is nucleated in each of the two free layers.

We note that if one were to analyze our device geometry in a simple macrospin picture for each of the free layers, one might expect to observe frequency doubling in the resistance signal, but for a completely different reason than the one indicated by the micromagnetic simulations. In a macrospin picture, the effect of the spin torque from the perpendicular polarizers would be to tilt one of the free layer magnetizations up relative to the sample plane and the other down, so that under the influence of their respective demagnetization fields (and in the absence of dipole coupling) one would precess clockwise about the z axis and the other counterclockwise. The relative angle between the layers and hence the resistance would therefore change at twice the precession frequency of either layer. The dynamics indicated by the micromagnetic simulations are different—the magnetic modes are strongly spatially nonuniform, and on average the moments of the two layers precess in the same direction [with a phase difference, see Fig. 4(b)] rather than in opposite directions.

To compare the micromagnetic computations to the experiments in more detail, we performed simulations at 300 K. The simulations exhibit current-driven steady-state magnetic oscillations for currents between $I_{dc} = 3.8$ and 5.9 mA. In this regime, the oscillation frequency, the linewidths, and the current dependence of the PSD amplitude calculated by the
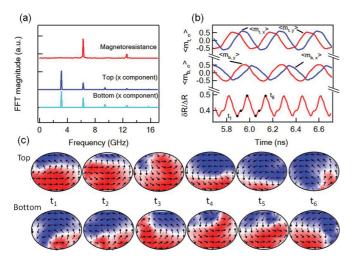

FIG. 4. (Color online) (a) Calculated power spectra for the magnetization oscillations in the top and bottom free layers and for the resistance oscillations of the full device at $I_{dc} = 5.3$ mA and zero external magnetic field. (b) Time traces for the calculated average x and y components of the magnetization oscillations in the top (m_t) and bottom (m_b) free layers, together with the calculated resistance oscillations. The black markers on the resistance oscillation indicate the six time points $t = t_1$ to t_6. (d) Micromagnetic configurations for the top and bottom free layers predicted by the micromagnetic simulation for the time points t_1 to t_6. The color scale represents the x component of the magnetization. The simulations in this figure correspond to zero temperature.

simulations [Figs. 3(a)–3(c), lower panels] in general agree well with the experimental peak A [Figs. 3(a)–3(c), upper panels], with no *ad hoc* manipulation of free parameters. The total amplitude of the time-dependent resistance signal is also in good agreement. For example, at $I_{dc} = 5.3$ mA the total amplitude of the resistance oscillation in the simulation is 12% of the full magnetoresistance ΔR for peak A, compared to the $\sim$7%–8% of ΔR output signal obtained in the experiment. There is some difference between simulation and experiment in the current dependence of the frequency. Experimentally we observe a slight redshift, while the simulations predict initially a slight blueshift with a redshift at larger currents. We find in the simulations that the current dependence of the frequency can vary between redshifts and blueshifts depending on the relative magnitudes of the spin-polarized currents arising from the two polarizers. Nevertheless, the room-temperature simulations confirm that the dynamics of the two free layers are phase locked to each other, and given the good semiquantitative agreement between the simulations and the experiment we believe that the simulations describe the essential features of the measurement well.

To further analyze the consequences of phase locking between the free layers, we performed a separate set of simulations for a simple spin valve geometry containing just a single Co free layer with one perpendicularly oriented polarizer layer [Fig. 3(d)]. In the absence of phase locking to a second free layer we obtain, as expected, precessional dynamics near 3 GHz, at half the frequency of the two-free-layer device. The linewidths for the single free layer are at least twice as broad as for the dynamics of two coupled free layers, suggesting that phase locking of the two free layers, in providing approximately a factor of 2 increase in effective

magnetic volume of the precessional mode, can improve the coherence of the magnetic oscillations.

In summary, we have explored the consequences of strong coupling between two magnetic free layers in spin-torque oscillators made with a hybrid structure consisting of two in-plane-oriented free layers sandwiched in between two perpendicularly oriented polarizer layers. We observe strong microwave output signals corresponding to phased-locked dynamics in the two free layers, with a fundamental frequency >6 GHz and a minimum linewidth of 74 MHz, without any externally applied magnetic field. Micromagnetic simulations reveal that the microwave output is due to spatially nonuniform magnetic dynamics in each of the two free layers. Our results suggest that phase locking can have several benefits for the quality of the resistance oscillations produced by the spin-torque oscillator: a doubling of the frequency above the precession frequency of each magnetic layer, a reduced linewidth compared to comparable devices with a single free layer, operation at zero magnetic field, and relatively large signals ($\sim$8% of the full ΔR, so that the power output of the device would be large when incorporated into a tunnel junction geometry).

[1] J. C. Slonczewski, J. Magn. Magn. Mater. **159**, L1 (1996).

[2] S. I. Kiselev, J. C. Sankey, I. N. Krivorotov, N. C. Emley, R. J. Schoelkopf, R. A. Buhrman, and D. C. Ralph, Nature (London) **425**, 380 (2003).

[3] M. Tsoi, A. G. M. Jansen, J. Bass, W. C. Chiang, M. Seck, V. Tsoi, and P. Wyder, Phys. Rev. Lett. **80**, 4281 (1998).

[4] W. H. Rippard, M. R. Pufall, S. Kaka, S. E. Russek, and T. J. Silva, Phys. Rev. Lett. **92**, 027201 (2004).

[5] A. M. Deac, A. Fukushima, H. Kubota, H. Maehara, Y. Suzuki, S. Yuasa, Y. Nagamine, K. Tsunekawa, D. D. Djayaprawira, and N. Watanabe, Nat. Phys. **4**, 803 (2008).

[6] D. Houssameddine, S. H. Florez, J. A. Katine, J.-P. Michel, U. Ebels, D. Mauri, O. Ozatay, B. Delaet, B. Viala, L. Folks, B. D. Terris, and M.-C. Cyrille, Appl. Phys. Lett. **93**, 022505 (2008).

[7] A. Slavin and V. Tiberkevich, IEEE Trans. Magn. **45**, 1875 (2009).

[8] M. R. Pufall, W. H. Rippard, M. L. Schneider, and S. E. Russek, Phys. Rev. B **75**, 140404 (2007).

[9] V. S. Pribiag, I. N. Krivorotov, G. D. Fuchs, P. M. Braganca, O. Ozatay, J. C. Sankey, D. C. Ralph, and R. A. Buhrman, Nat. Phys. **3**, 498 (2007).

[10] Q. Mistral, M. van Kampen, G. Hrkac, Joo-Von Kim, T. Devolder, P. Crozat, C. Chappert, L. Lagae, and T. Schrefl, Phys. Rev. Lett. **100**, 257201 (2008).

[11] A. Ruotolo, V. Cros, B. Georges, A. Dussaux, J. Grollier, C. Deranlot, R. Guillemet, K. Bouzehouane, S. Fusil, and A. Fert, Nat. Nanotechnol. **4**, 528 (2009).

[12] S. Kaka, M. R. Pufall, W. H. Rippard, T. J. Silva, S. E. Russek, and J. A. Katine, Nature (London) **437**, 389 (2005).

[13] F. B. Mancoff, N. D. Rizzo, B. N. Engel, and S. Tehrani, Nature (London) **437**, 393 (2005).

[14] See Supplemental Material at http://link.aps.org/supplemental/10.1103/PhysRevB.86.060411 for details about the sample fabrication, measurement techniques, and the micromagnetic simulations.

[15] D. Houssameddine, U. Ebels, B. Delaët, B. Rodmacq, I. Firastrau, F. Ponthenier, M. Brunet, C. Thirion, J.-P. Michel, L. Prejbeanu-Buda, M.-C. Cyrille, O. Redon, and B. Dieny, Nature Mater. **6**, 447 (2007).

[16] W. H. Rippard, A. M. Deac, M. R. Pufall, J. M. Shaw, M. W. Keller, S. E. Russek, G. E. W. Bauer, and C. Serpico, Phys. Rev. B **81**, 014426 (2010).

[17] S. M. Mohseni, S. R. Sani, J. Persson, T. N. Anh Nguyen, S. Chung, Ye. Pogoryelov, and J. Åkerman, Phys. Status Solidi (RRL) **5**, 432 (2011).

[18] G. Finocchio, V. S. Pribiag, L. Torres, R. A. Buhrman, and B. Azzerboni, Appl. Phys. Lett. **96**, 102508 (2010).

[19] G. Finocchio, I. N. Krivorotov, L. Torres, R. A. Buhrman, D. C. Ralph, and B. Azzerboni, Phys. Rev. B **76**, 174408 (2007).

[20] C. Kaiser, S. van Dijken, S.-H. Yang, H. Yang, and S. S. P. Parkin, Phys. Rev. Lett. **94**, 247203 (2005). We use the value for $Co_{0.25}Pt_{0.75}$ alloy.

[21] D. Ravelosona, S. Mangin, Y. Henry, Y. Lemaho, J. A. Katine, B. D. Terris, and E. E. Fullerton, J. Phys. D: Appl. Phys. **40**, 1253 (2007). We estimate the Co/Ni spin polarization by comparing the magnetoresistance of Co/Ni and Co/Pt spin valves.

[22] P. M. Tedrow and R. Meservey, Phys. Rev. B **7**, 318 (1973).